Micro- and Nanocubes of Silicon with Zinc-Blende Structure

P. Liu, Y. L. Cao, H. Cui, X. Y. Chen, and G. W. Yang*

State Key Laboratory of Optoelectronic Materials and Technologies, Institute of Optoelectronic and Functional Composite Materials, School of Physics Science & Engineering, Zhongshan University, Guangzhou 510275, P. R. China

Received September 22, 2007. Revised Manuscript Received November 7, 2007

Micro- and nanocubes of single-crystalline silicon with the zinc-blende structure have been synthesized by pulsed-laser-induced liquid–solid interface reaction. Raman scattering, scanning electron microscopy, transmission electronic microscopy equipped with energy dispersive X-ray spectrometer, selected area electron diffraction, and electron energy-loss spectroscopy are employed to characterize the morphology and structure of the as-synthesized samples. The first-principles calculations are employed to theoretically analyze the data of experiments. The synthesis mechanisms of silicon cubes upon PLIIR are pursued in physical and chemical mechanisms.

I. Introduction

Intensive research of inorganic nanomaterials had been extensively devoted and described since the past century due to their unique applications in mesoscopic chemistry, physics, and fabrication of nanodevices.[1,2] In recent years, the morphology-controlled synthesis of nanoparticles has been one of the frontier fields in nanomaterials science and technology because the shape and size of low-dimensional structures play crucial roles in the chemical and physical properties of materials.[3–5] Consequently, considerable efforts have been made for the controlling synthesis of nanomaterials with desired structure or morphology in the past years.[6,7] Numerous nanostructures such as nanorods, nanobelts, nanowires, nanorings, and other nanoconfigurations with interesting morphologies or specific structures have been successfully synthesized.[8–14] Similarly, nanocubes with wide applications have attracted special interest from both theoretical and applicable perspectives due to their shape-dependent properties.[15–20] Many techniques have been developed to synthesize nanocubes including colloidal self-assemblies mode, HTAB-modified reaction, epitaxial electrodeposition, hydrothermal treatment, and so on.[21–27] For instance, Xia et al.[18,28–39] have done intensive research in the synthesis of nanocubes of noble metals. However, only

* Corresponding author: e-mail stsygw@mail.sysu.edu.cn.

(1) Wang, Z. L. *Adv. Mater.* **2003**, *15*, 1497.
(2) Liu, Q. X.; Wang, C. X.; Yang, Y. H.; Yang, G. W. *Appl. Phys. Lett.* **2004**, *84*, 4568.
(3) Puntes, V. F.; Krishnan, K. M.; Alivisatos, A. P. *Science* **2001**, *291*, 2115.
(4) Jana, N. R.; Gearheart, L.; Obare, S. O.; Murphy, C. J. *Langmuir* **2002**, *18*, 922.
(5) Feng, X.; Sayle, D. C.; Wang, Z. L.; Paras, M. S.; Santora, B.; Sutorik, A. C.; Sayle, T. X. T.; Yang, Y.; Ding, Y.; Wang, X.; Her, Y. S. *Science* **2006**, *312*, 1504.
(6) Xia, Y.; Yang, P.; Sun, Y.; Wu, Y.; Mayers, B.; Gates, B.; Yin, Y.; Kim, F.; Yan, H. *Adv. Mater.* **2003**, *15*, 353.
(7) Cao, M.; Liu, T.; Gao, S.; Sun, G.; Wu, X.; Hu, C.; Wang, Z. L. *Angew. Chem.* **2005**, *117*, 4269.
(8) Wang, J.; Huang, H.; Kesapragada, S. V.; Gall, D. *Nano Lett.* **2005**, *5*, 2505.
(9) Pan, Z. W.; Dai, Z. R.; Wang, Z. L. *Science* **2001**, *291*, 1947.
(10) Orlandi, M. O.; Leite, E. R.; Aguiar, R.; Bettini, J.; Longo, E. *J. Phys. Chem. B* **2006**, *110*, 6621.
(11) Martensson, T.; Svensson, C. P. T.; Wacaser, B. A.; Larsson, M. W.; Seifert, W.; Deppert, K.; Gustafsson, A.; Wallenberg, L. R.; Samuelson, L. *Nano Lett.* **2004**, *4*, 1987.
(12) Cho, K. S.; Talapin, D. V.; Gaschler, W.; Murray, C. B. *J. Am. Chem. Soc.* **2005**, *127*, 7140.
(13) Ding, Y.; Ma, C.; Wang, Z. L. *Adv. Mater.* **2004**, *16*, 1740.
(14) Gao, P. X.; Ding, Y.; Mai, W.; Hughes, W. L.; Lao, C.; Wang, Z. L. *Science* **2005**, *309*, 1700.
(15) Murphy, C. J. *Science* **2002**, *298*, 2139.
(16) Sosa, I. O.; Noguez, C.; Barrera, R. G. *J. Phys. Chem. B* **2003**, *107*, 6269.
(17) Chan, E. R.; Zhang, X.; Lee, C. Y.; Neurock, M.; Glotzer, S. C. *Macromolecules* **2005**, *38*, 6168.
(18) Sun, Y.; Xia, Y. *Science* **2002**, *298*, 2176.
(19) Dumestre, F.; Chaudret, B.; Amiens, C.; Renaud, P.; Fejes, P. *Science* **2004**, *303*, 821.
(20) Sherry, L. J.; Chang, S. H.; Schatz, G. C.; Van Duyne, R. P.; Wiley, B. J.; Xia, Y. *Nano Lett.* **2005**, *5*, 2034.
(21) Pileni, A.; Filankembo, M. P. *J. Phys. Chem. B* **2000**, *104*, 5865.
(22) Yu, D.; Yam, V. W. W. *J. Am. Chem. Soc.* **2004**, *126*, 13200.
(23) Xiong, Y.; Chen, J.; Wiley, B.; Xia, Y.; Yin, Y.; Li, Z. Y. *Nano Lett.* **2005**, *5*, 1237.
(24) Liu, R.; Oba, F.; Bohannan, E. W.; Ernst, F.; Switzer, J. A. *Chem. Mater.* **2003**, *15*, 4882.
(25) Mao, Y.; Banerjee, S.; Wong, S. S. *J. Am. Chem. Soc.* **2003**, *125*, 15718.
(26) Siegfried, M. J.; Choi, K. S. *Adv. Mater.* **2004**, *16*, 1743.
(27) Xiong, Y.; Wiley, B.; Chen, J.; Li, Z. Y.; Yin, Y.; Xia, Y. *Angew. Chem.* **2005**, *117*, 8127.
(28) Xiong, Y.; Chen, J.; Wiley, B.; Xia, Y.; Yin, Y.; Li, Z. Y. *Nano Lett.* **2005**, *5*, 1237.
(29) Im, S. H.; Li, Y. T.; Wiley, B.; Li, Z. Y.; Xia, Y. *Angew. Chem., Int. Ed.* **2005**, *44*, 2154.
(30) Matsumoto, H.; Higuchi, K.; Kyushin, S.; Goto, M. *Angew. Chem., Int. Ed. Engl.* **1992**, *31*, 1354.
(31) Motiei, M.; Calderon-Moreno, J.; Gedanken, A. *Adv. Mater.* **2002**, *14*, 1169.
(32) Wang, W.; Huang, J.; Ren, Z. *Langmuir* **2005**, *21*, 751.
(33) Robertson, J. *Mater. Sci. Eng., R* **2002**, *37*, 129.
(34) Belomoin, G.; Therrien, J.; Smith, A.; Rao, S.; Twesten, R.; Chaieb, S.; Nayfeh, M. H.; Wagner, L.; Mitas, L. *Appl. Phys. Lett.* **2002**, *80*, 841.
(35) Li, A. P.; Flack, F.; Lagally, M. G.; Chisholm, M. F.; Yoo, K.; Zhang, Z.; Weitering, H. H.; Wenderlken, J. F. *Phys. Rev. B* **2004**, *69*, 245–310.
(36) Yang, G. W. *Prog. Mater. Sci.* **2007**, *52*, 648.
(37) Yang, G. W.; Wang, J. B. *Appl. Phys. A: Mater. Sci. Process.* **2001**, *72*, 475.
(38) Liu, Q. X.; Wang, C. X.; Zhang, W.; Yang, G. W. *Chem. Phys. Lett.* **2003**, *382*, 1.
(39) Wiley, B.; Herricks, T.; Sun, Y.; Xia, Y. *Nano Lett.* **2004**, *4*, 1733.

10.1021/cm7027178 CCC: $40.75
Published on Web 12/19/2007

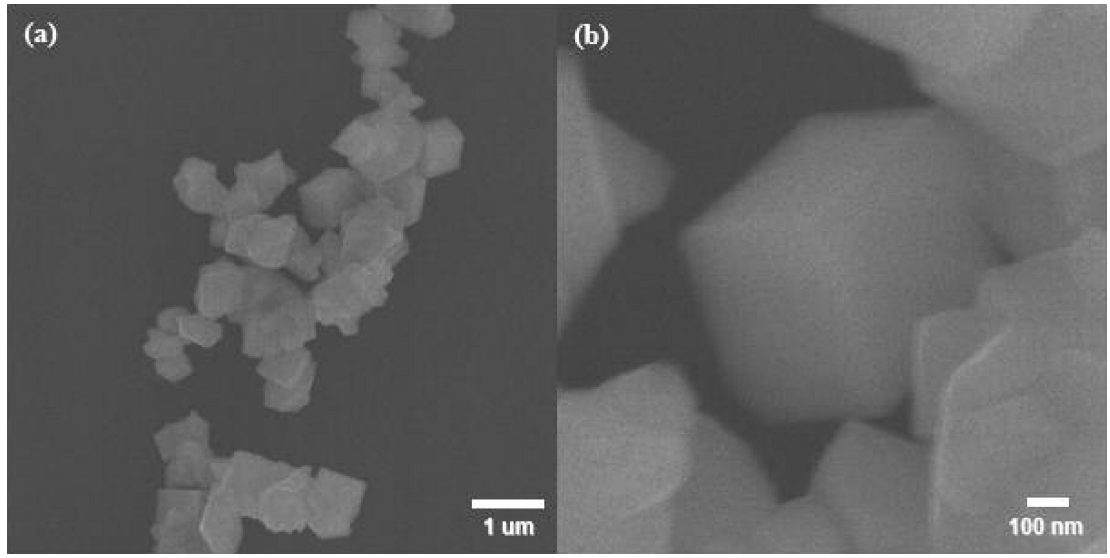

Figure 1. SEM images of the synthesized silicon cubes: (a) low magnification and (b) high magnification.

metal, metal-associated material, or oxide material nanocubes have been synthesized, and there have been too few studies involved in the semiconductor nanocubes in the present securable literature.[18–32] It is well-known that many fields would greatly benefit from the advances in the synthesis of well-defined nanostructures, including photonics, information storage, nanoelectronics, catalysis, and biosensors.[33–35] Therefore, it is a great challenge to develop a new synthetic method for the shape-controlled synthesis of semiconductor nanocubes. In this contribution, we report that the unique micro- and nanocubes of single-crystalline silicon with the zinc-blende structure are, for the first time, synthesized by pulsed-laser-induced liquid–solid interface reaction (PLIIR). Additionally, the physical and chemical mechanisms of the silicon cubes synthesis upon PLIIR are discussed in this contribution.

II. Experimental Section

The detailed PLIIR synthesis has been reported in our previous works.[36–38] In this case, the solid target is a single-crystalline silicon substrate deposited the amorphous carbon layer with the thickness of 100–300 nm by a filtered cathode vacuum arc (FCVA) technique with the pressure of 3×10^{-5} Torr and the substrate temperature of 300 K. The liquid, which is used as assistant agents in our synthesis, is selected to be a mixture of the twice-distilled water, ethanol, acetone, and very low concentration inorganic salts solutions (below <8 mM) such as KCl and NaCl solutions. Note that our motivation lies specifically in utilizing simple inorganic ions as additives instead of surfactant molecules or organic molecules. In general, inorganic ions have a more pronounced influence on the nucleation process of crystals than that of organic surfactants or polymers.[21,39] All aqueous solutions that are used as the laser ablation environments are prepared from the twice-distilled water, KCl (99.5+%), and NaCl (99.5+%), and the concentration ratio of the twice-distilled water, ethanol, acetone, and inorganic salt is about 5:2.5:1.5:1. A second-harmonic laser is produced by a Q-switched Nd:YAG laser with wavelength of 532 nm, pulse width of 10 ns, power density of 10^{10} W/cm^2, and repetition rate of 10 Hz. The synthesis is described as follows. The solid target is first fixed on the bottom of a quartz chamber. Then, the liquid is poured slowly into the chamber until the target is covered by 2–3 mm. Finally, the pulsed laser is focused onto the surface of the solid target (an ablation rate of about 10–20 nm/pulse can be obtained in our case[36]). During the laser ablating, the target and liquid are maintained at room temperature. Meanwhile, the target rotates or moves horizontally at a slow speed. After the pulsed-laser interacted with the target for 15−20 min, the solid target is taken out and dried from the liquid. Note that, in our case, the surface of silicon targets is covered by the synthesized products, which is the sample to be used in the characterizations below. Before measuring, these samples are washed and dialyzed carefully with the deionized water for 1 h to remove the remaining inorganic salts and then dried at 60 °C again in an oven.

The scanning electron microscopy (SEM) images of the as-synthesized samples are obtained by a JSM-6330F filed emission scanning electron microscope operated at 15 kV. The Raman spectrum of samples is recorded on a Renishaw inVia+Plus laser micro-Raman spectrometer with detected Ar ion laser irradiation of $\lambda = 514.5$ nm. The transmission electron microscopy (TEM) images of samples and the corresponding selected area electron diffraction (SAD) patterns are taken by a JEOL JEM-2010H transmission electron microscope. A JEM-2010F transmission electron microscope operated at 200 kV is used to measure the high-resolution TEM (HRTEM) image and the EELS spectra of samples.

III. Results and Discussion

A. Morphology, Composition, and Structure of Products. Figure 1 shows SEM images of the typical as-synthesized samples; the corresponding EDS attached SEM indicates that the synthesized product is composed of silicon element within the measurement error of 4%. Considering that some surfaces of the single-crystalline silicon target are roughened by the laser ablation, we measure the samples that are deposited on the local glazed surface of the substrate. Therefore, the observed products are distinguished clearly from the background. Additionally, our studies clarify that the roughened surfaces of the substrate have a slight influence on the nanoparticle growth. Interestingly, we can clearly see the as-synthesized samples are cubes in the high-magnification SEM image of Figure 1b, and these cubes have perpendicular fringes that are either parallel to or orthogonal to the upright facet of cubes. The side length of these cubes is in the

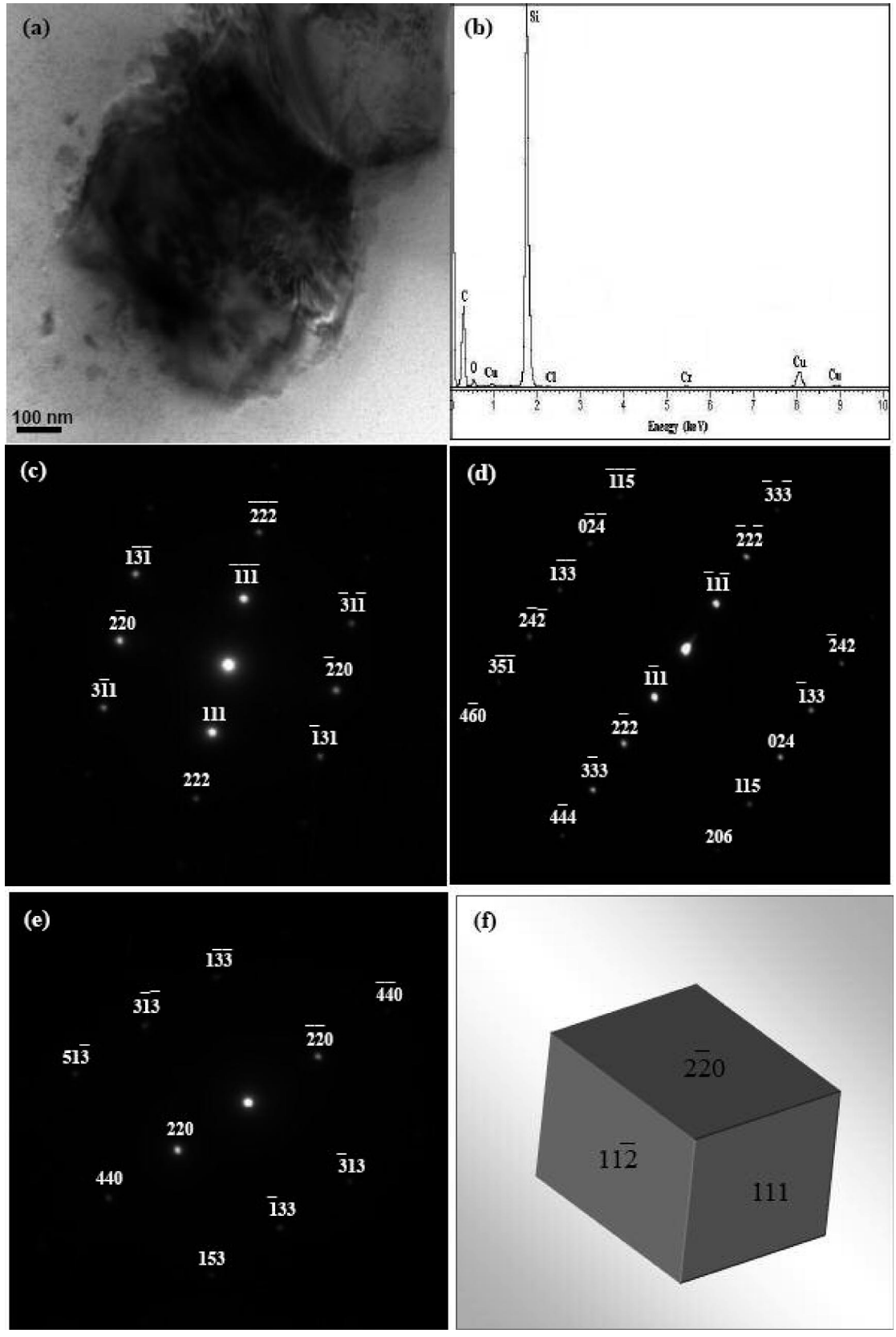

Figure 2. TEM image (a), the corresponding EDS spectrum (b), and the corresponding SAD patterns (c−e) of a single silicon cube. (f) A model of the silicon cube that was rebuilt on the basis of the SAED analysis.

range 200–500 nm. Therefore, these primal results show that the synthesized samples are micro- and nanocubes of silicon.

A JEOL JEM-2010H TEM operated at 200 kV is employed to measure the bright-field images and the corresponding SAD patterns of the samples. Figure 2a shows a bright-field image of samples, and the corresponding EDS spectrum within the measurement error of 2% is shown in Figure 2b. Thus, these results undoubtedly indicate that the synthesized cubes are pure

Table 1. Indexing Results of SAD Patterns of Micro- and Nanocubes, with the Comparison of the Experimental Data of Zinc-Blende and Diamond-Type Structures of Silicon[a]

(*hkl*)	D_{exp} (Å)	$D_{calc,zb}$ (Å)[b]	$D_{calc,d}$ (Å)[c]
111	3.1063	3.1130	3.1355
131	1.6291	1.6257	1.6374
133	1.2366	1.2370	1.2458
220	1.9002	1.9063	1.9201
222	1.5537	1.5565	1.5677
242	1.0998	1.1006	1.1085
311	1.6304	1.6257	1.6374
422	1.1002	1.1006	1.1085

[a] D_{exp} refers to our experimental values, $D_{calc,zb}$ refers to the predicted values of zinc-blende structure, and $D_{calc,d}$ refers to the predicted values of diamond structure.[18,19] [b] JCPDS Card File No. 800018. [c] JCPDS Card File No. 895012.

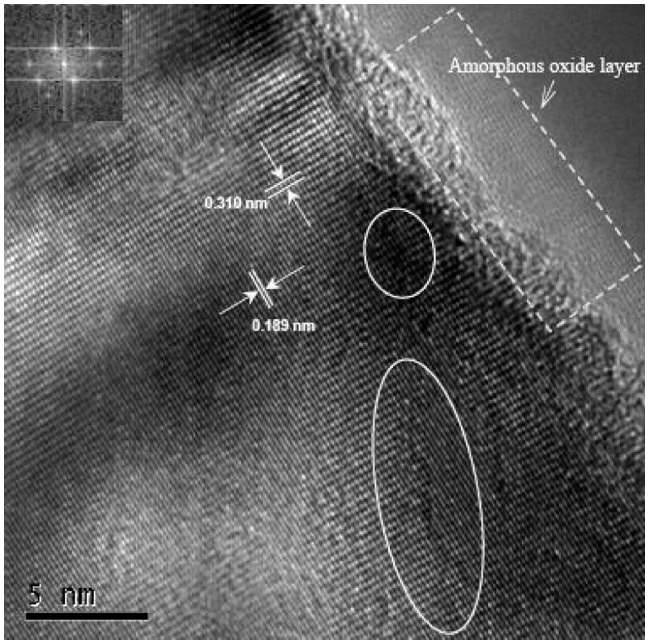

Figure 3. HRTEM image of an edge of a single silicon cube. The inset is the corresponding fast Fourier transform (FFT) analysis.

silicon. In Figure 2b, the Cu, Cr, and C peaks originate from the copper grid and the amorphous carbon film support, while the very slight Cl peak comes from the impurity and the weak O peak is supposed to come from the amorphous carbon film support or the exterior oxide layer of the Si cubes.

Three corresponding selected area electron diffraction (SAD) patterns of silicon cubes are shown in Figure 2c−e. The representative SAD patterns are obtained by directing the electron beam perpendicular to the different crystal facets of the cube shown in Figure 2a. These SAD patterns reveals that the synthesized silicon cubes are single crystal and are bounded mainly by two {111} facets, two {220} facets, and two {112} facets. These results are schematically illustrated in Figure 2f. Additionally, we calculate the d_{exp} values of silicon cubes from the SAD patterns. Table 1 lists a comparison of the experimental data of silicon cubes, the calculated value of the zinc-blende structure of silicon (JCPDS Card File No. 800018), and the value of the single-crystalline silicon with diamond structure (JCPDS Card File No. 895012).[40,41] Clearly, the d_{exp} values of silicon cubes are well consistent with the theoretical d_{calc} value of the zinc-blende structure of silicon. Therefore, these results show that the synthesized cubes are single-crystalline silicon with the zinc-blende structure.

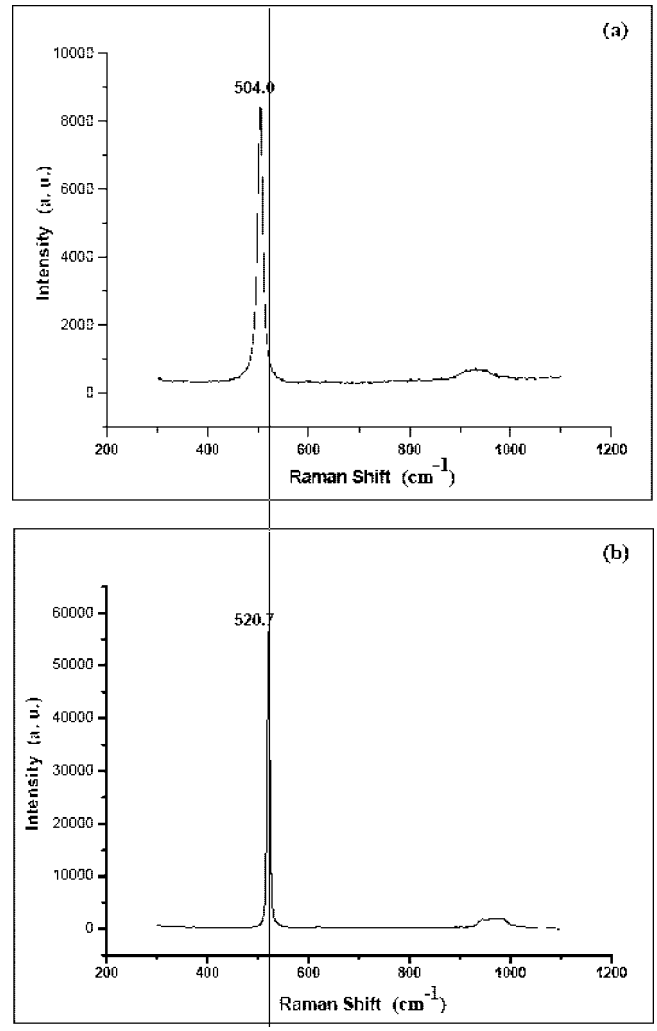

Figure 4. (a) Raman spectrum of silicon cubes with detected laser energy of 1 mW. (b) Raman spectrum of the silicon substrate.

A JEM-2010F TEM operated at 200 kV is employed to measure the HRTEM image and the corresponding EEL spectra of samples. Figure 3 shows a HRTEM image of one facet of the silicon cube. A careful examination indicates that the interplanar spacings of the cube is 0.310 and 0.189 nm, which are both smaller than the *d* values of the diamond structural crystalline silicon but well in agreement with the d_{calc} value of [111] and [220] of the zinc-blende structure of silicon. A fast Fourier transform (FFT) analysis (the inset in Figure 3) shows the square spot array of the 2D lattice fringes, which can just be indexed to the (111) and (220) directions. Moreover, we can see a thin amorphous layer on the outer surface of the silicon cube indicated by a dashed square. This result shows that the silicon cube is covered with a thin amorphous oxide layer, which leads to the O peak in the EDS spectrum (Figure 2b). Note that there are some saturated regions in the lattice planes (marked with white circles). This result implies that there should be some

(40) Yeh, C. Y.; Lu, Z. W.; Froyen, S.; Zunger, A. *Phys. Rev. B* **1992**, *46*, 10086.
(41) Straumanis, M. E.; Aka, E. Z. *J. Appl. Phys.* **1952**, *23*, 330.

asymmetrical lattice structures in the cube,[42] which is suspected to be caused by inner defects or slight dislocations.

B. Raman and EELS Spectra of Si Cubes. Figure 4a shows the corresponding Raman spectrum of the sample, while the Raman spectrum of the single-crystalline silicon substrate is shown in Figure 4b. Definitely, there are two different Raman peaks in Figure 4: one peak at 504 cm^{-1} is from the as-synthesized sample, and the other peak at 520 cm^{-1} is from the single-crystalline silicon substrate. Thus, there is an obvious Raman shift between the silicon cubes and the single-crystalline silicon substrate. Usually, Si nanocrystals have a Raman shift because of the quantum size effect or the heating by the visible laser.[43,44] However, in our case, the size of silicon cubes seems far beyond the quantum size effect regime. In addition, the energy of the detected laser is only set to be 1 mW. Therefore, the Raman shift of silicon cubes is not attributed to the quantum size effect or laser heating effect. According to the HRTEM image (Figure 3), this Raman shift seems to originate from the crystalline defects; i.e., there is the inner stress in these silicon cubes. First, the cubic shape is not a natural morphology of single-crystalline silicon particle; thus, there would be some inner energy or lattice stress in the silicon cube, which may be caused by the lattices mismatch or distorted, and not be released completely. Second, PLIIR is a very fast process, i.e., far beyond thermodynamic equilibrium; thus, these silicon cubes from PLIIR are usually a metastable phase. Therefore, some defects can form in the synthesized samples as shown in Figure 3. Moreover, some theoretical calculations show that the cubic morphology would induce the spectral shifts.[45] Accordingly, the Raman peak at 504 cm^{-1} seems to be the intrinsic Raman peak of the silicon cubes with the zinc-blende structure.

Figure 5 shows the electron energy loss spectrum (EELS) of the as-synthesized sample, in which parts a and b of Figure 5 show a low-loss spectrum and a high-loss spectrum of the samples, respectively. Meanwhile, standard low-loss and high-loss spectra of the diamond structure crystalline silicon are exhibited in Figure 5c,d. In the low-loss spectra, we can see that the main plasmon peak in Figure 5a is located at around 17 eV, which is in well agreement with that shown in Figure 5c. This result indicates that the synthesized silicon cubes are single-crystalline silicon. A stretching mode after 17 eV shown in Figure 5a seems different from that shown in Figure 5c because the standard spectrum exhibits only one single and broad plasmon peak at 17 eV in Figure 5c. Thus, this stretching mode at about 21 eV shown in Figure 5a is suggested to be attributed to the zinc-blende silicon. In the high-loss spectra, we confirm that the plasmon peak at 101.5 eV shown in Figure 5b is in agreement with the peak at 101 eV shown in Figure 5d, which is the L-edge absorption peak of crystalline silicon. Then, the second plasmon peak shown in Figure 5b is at 104 eV, which is different from the second plasmon peak at 108 eV in Figure 5d.

Considering that the fine structure of a sample can be inspected in the high-loss spectrum, the peak shift of Figure 5b indicates that there is a difference between the crystalline structures of silicon cube and single-crystalline silicon with diamond structure. To clarify this issue, we carry out the first-principle calculations to theoretically determine the EEL spectrum (low loss) of the zinc-blende structure and diamond structure of silicon, and the calculated results are shown in Figure 5e. In Figure 5e, the black solid line represents the zinc-blende structure, and the red dash-dotted line represents the diamond structure. In our calculations, an accurate full-potential, linearized, augmented plane wave method is used, and the exchange and correlation effects are treated within the generalized gradient approximation (GGA).[46] The muffin-tin sphere of silicon is set to $R = 2.1$ for zinc-blende structure and $R = 1.25$ for diamond structure. Note that, for the zinc-blende structure, a mesh of $10 \times 10 \times 10$ is used to represent 47K points in the irreducible wedge of Brillouin zone. Comparing parts a and c of Figure 5 with part e, we can see that there is indeed a difference between the zinc-blende and diamond structures of silicon in the low-loss spectrum. In detail, the red dash-dotted line spectrum in our calculations exhibits only one single plasmon peak at 17 eV, which is in well agreement with the standard spectrum shown in Figure 5c. Meanwhile, the black solid line spectrum depicted in Figure 5e indicates not only a plasmon peak at 17 eV but also a skew stretching mode after 17 eV, which is at about 19 eV and is very similar to that shown in Figure 5a. Considering that the calculated value would have little difference to the actual value, these results confirm that the synthesized cubes are the zinc-blende structure of silicon.

On the basis of experimental analyses of SAD, HRTEM, EELS, and theoretical results by the first-principle calculations, we can conclude that the synthesized cubes are single silicon with the zinc-blende structure, which is indeed different from the diamond structure of silicon.

C. Comparison of Different Experimental Cases. We carry out the different syntheses under the different liquid environments, and the results are shown in Figure 6. Clearly, in Figure 6a, we can see that all the products are spherical-like particles with the average size of about 400–600 nm, when the liquid environment is the twice-distilled water. Similarly, in Figure 6b, we can see that most of the products are spherical-like particles, when the liquid environments are the different inorganic salts solutions. Then, there are some nonspherical particles in the products, which imply that the inorganic salts have effects on the shape formation of the products. Figure 6c shows the morphology of the products from the laser ablation of silicon targets with amorphous carbon layer in the twice-distilled water. Interestingly, we can see that many particles are rather regular sphere (non spherical) with the size in the range of 300–400 nm. Thus, these particles are smaller than that of the products synthesized in the twice-distilled water shown in Figure 6a. Therefore, the amorphous carbon layer has influence on the shape formation of the products. By comparing three kinds of the products synthesized in three

(42) Wang, Z. L. *Part. Part. Syst. Charact.* **2001**, *18*, 142.
(43) Zhang, S. L.; Hou, Y.; Ho, K. S.; Qian, B.; Cai, S. *J. Appl. Phys.* **1992**, *72*, 4469.
(44) Poborchii, V.; Tada, T.; Kanayama, T. *J. Appl. Phys.* **2005**, *97*, 104323.
(45) Wiley, B. J.; Im, S. H.; Li, Z. Y.; McLellan, J.; Siekkinen, A.; Xia, Y. *J. Phys. Chem. B* **2006**, *110*, 15666.
(46) Perdew, J. P.; Burke, K.; Ernzerhof, M. *Phys. Rev. Lett.* **1996**, *77*, 3865.

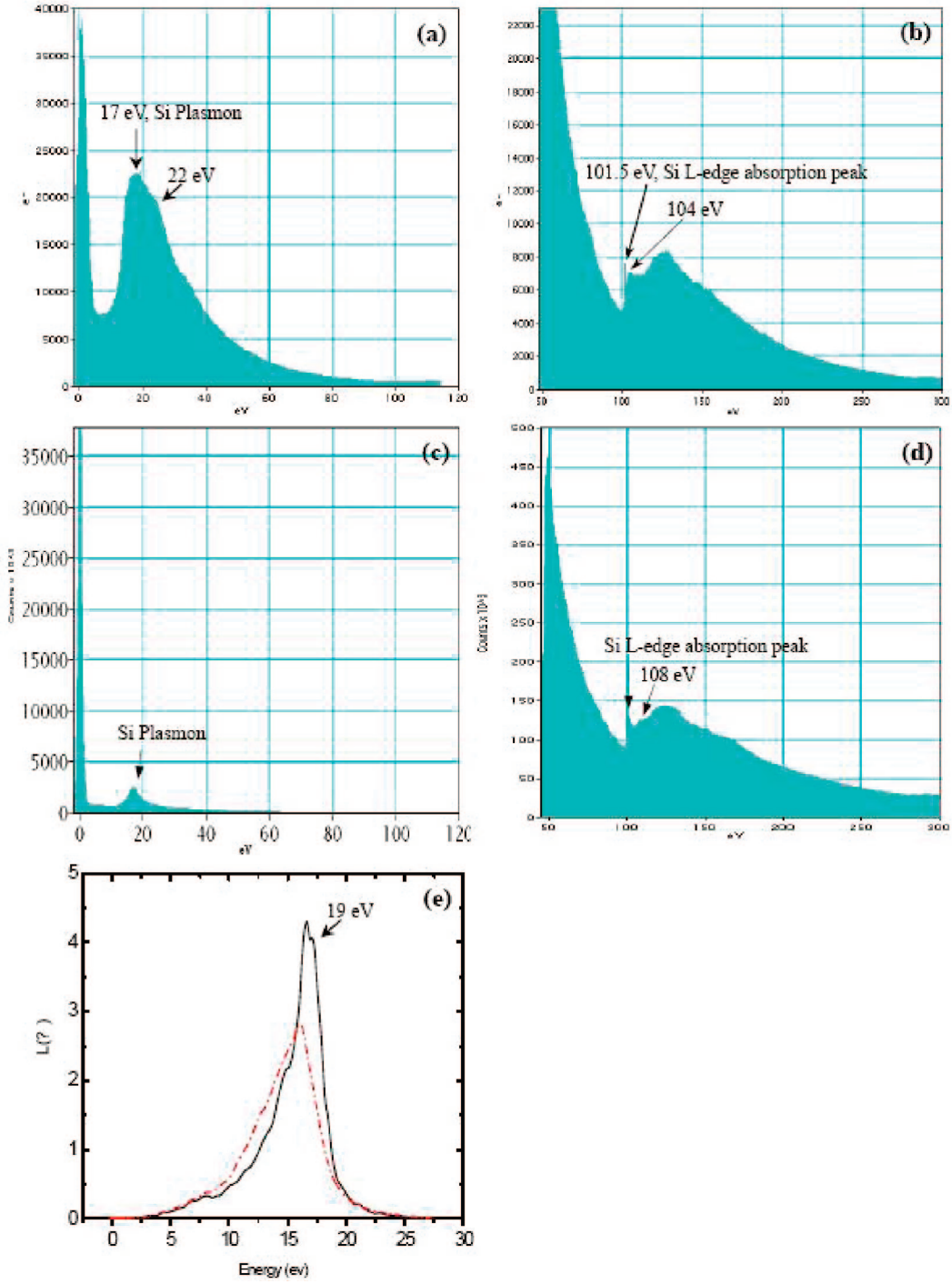

Figure 5. (a) Low-loss and (b) high-loss spectra of EELS of samples. (c) Low-loss and (d) high-loss spectra of the standard diamond structure of silicon. (e) Theoretical calculated EELS (low-loss) of the silicon with the zinc-blende and diamond structures through the first-principles method.

different liquid environments, we can conclude that the amorphous carbon layer and inorganic salts have effects on the size and shape formation of silicon cubes in the PLIIR synthesis.

D. Growth Mechanism. It is well-known that PLIIR is a very fast and far from thermodynamic equilibrium process. Thus, all stable and metastable phases forming at the initial, the intermediate, and the final stages of the synthesis process may be reserved in the final products, especially the metastable intermediate phase.[47–49] For instance, two structures, i.e., the metastable hexagonal and stable cubic structure of diamonds, have been observed simultaneously in the same sample synthesized by

(47) Berthe, L.; Fabbro, R.; Peyer, P.; Tollier, L.; Bartnicki, E. *J. Appl. Phys.* **1997**, *82*, 2826.
(48) Berthe, L.; Fabbro, R.; Peyer, P.; Bartnicki, E. *J. Appl. Phys.* **1999**, *85*, 7552.
(49) Sollier, A.; Berthe, L.; Fabbro, R. *Eur. Phys. J. Appl. Phys.* **2001**, *16*, 131.
(50) Yang, G. W.; Wang, J. B.; Liu, Q. X. *J. Phys.: Condens. Matter* **1998**, *10*, 7923.
(51) Wang, J. B.; Zhang, C. Y.; Zhong, X. L.; Yang, G. W. *Chem. Phys. Lett.* **2002**, *361*, 86.

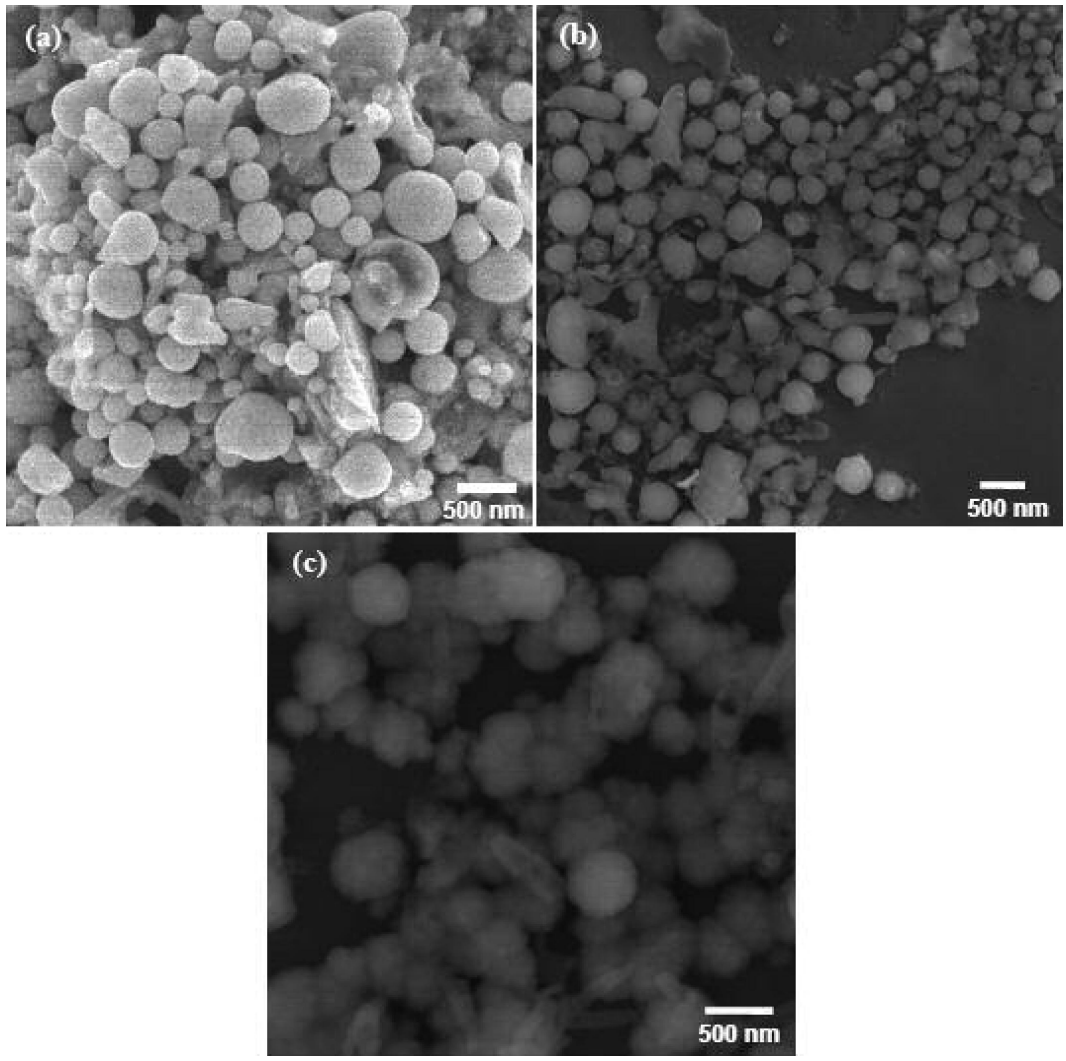

Figure 6. Products synthesized in the twice-distilled water (a) and the different inorganic salts solutions (b). (c) Products from laser ablation of silicon targets with amorphous carbon layer in the twice-distilled water.

PLIIR.[50,51] Following Fabbro's studies, at the initial stage of laser ablation in liquid, a large number of species having large initial kinetic energy eject from the solid target surface and form a dense region, i.e., a laser-induced plasma plume, in the vicinity of the solid–liquid interface due to the confinement effect of liquid.[47–49] Then, the laser energy is greatly spent in mechanical or dynamical effects in laser ablation in liquid environments.[52,53] Since the plasma plume is strongly confined in the liquid, the liquid would stop the plasma plume expansion to form an adiabatic region,[54] in which a shock wave will be created at supersonic velocity in front, and it will induce an extra pressure, called laser-induced pressure, in the plasma plume. Further, the laser-induced pressure leads to a temperature increasing in the plasma plume. Therefore, the plasma plume created in the duration of pulsed-laser ablation at liquid–solid interface is in the higher temperature, higher pressure, and higher density (HTHPHD) state. For example, in the case of laser ablation of graphite in water, the temperature is about 4000–5000 K and the pressure is about 10–15 GPa.[55] Thus, the high-amplitude stress waves would be applied on the solid target, while the phase transition between species in the plasma plume would happen.[56] As a result of the strong confinement effect of liquid, the quenching time of the plasma plume in the liquid becomes so short that the metastable phase forming at the intermediate stage of the synthesis could be frozen in the synthesized final products. In addition, the laser fluence plays an important role in controlling phase formation upon PLIIR; i.e., the different laser fluences could result in forming the different metastable phases.[57,58]

For our case, the laser-induced plasma plume is first generated at the liquid–solid interface when pulsed-laser ablating the solid target. Since there are amorphous carbons covered the silicon target, the plasma plume

(52) Zhu, S.; Lu, Y. F.; Hong, M. H.; Chen, X. Y. *J. Appl. Lett.* **2001**, *89*, 2400.
(53) Giacomo, A. D.; Dell'Aglio, M.; Colao, F.; Fantoni, R. *Spectrochim. Acta, Part B* **2004**, *59*, 1431.
(54) Wang, C. X.; Liu, P.; Cui, H.; Yang, G. W. *Appl. Phys. Lett.* **2005**, *87*, 201913.
(55) Wang, J. B.; Yang, G. W. *J. Phys: Condens. Matter* **1999**, *11*, 7089.
(56) Ashfold, M. N. R.; Claeyssens, F.; Fuge, G. M.; Henley, S. J. *Chem. Soc. Rev.* **2004**, *33*, 23.
(57) Patil, P. P.; Phase, D. M.; Kulkarni, S. A.; Ghaisas, S. V.; Kulkarni, S. K.; Kanetkar, S. M.; Ogale, S. B. *Phys. Rev. Lett.* **1987**, *58*, 238.
(58) Ogale, S. B.; Patil, P. P.; Phase, D. M.; Bhandarkar, Y. V.; Kulkarni, S. K.; Kulkarni, S.; Ghaisas, S. V.; Kanetkar, S. M. *Phys. Rev. B* **1987**, *36*, 8237.

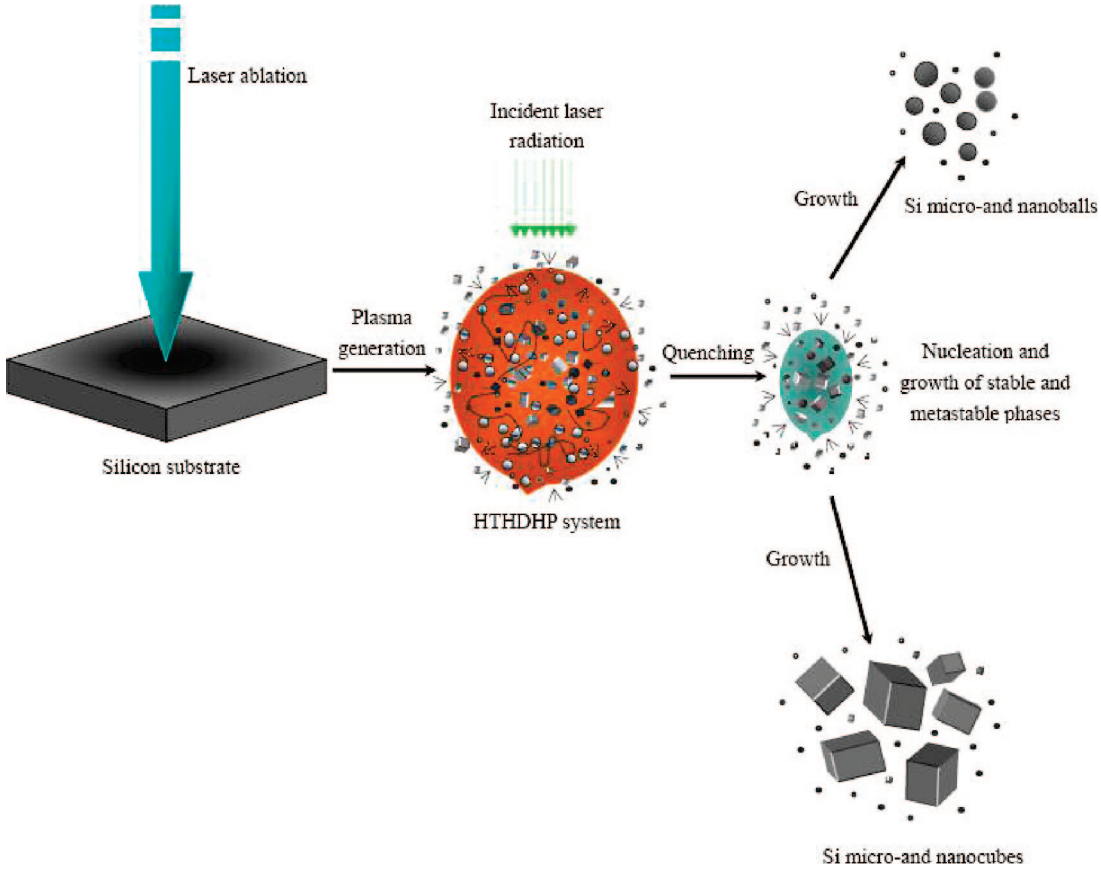

Figure 7. Schematic illustration of the synthesis mechanisms of silicon cubes upon PLIIR.

contains silicon and carbon species from the target and the salt ions from the liquid. Then, the expansion of the plasma plume will be delayed due to the confinement of liquid. Thus, the laser-induced pressure would be an order of magnitude greater, and the shock wave duration would be 2–3 times longer than that in the direct regime at the same power density.[47] Therefore, the incident laser radiation and the laser-induced pressure would drive the plasma plume into the HTHPHD state,[56] in which silicon species will impact with each other drastically to form the stable and mestable phase.

The phase transition from the diamond to zinc-blende structures of silicon maybe take place in the plasma plume with the HTHPHD state. As we know, the silicon with the zinc-blende structure is a metastable phase compared with the diamond structural silicon. Therefore, the diamond structural silicon is energetically preferable to the zinc-blende silicon in thermodynamics. However, PLIIR is a far from thermodynamic equilibrium process, which provides many opportunities to the formation of metastable phases.[36–38] For example, the intermediate rhombohedral graphite is observed in the pulsed-laser induced phase transformation, and the geometric path of the phase transition of graphite-to-rhombohedral graphite is proposed in our previous work.[59] Therefore, some silicon species with the diamond structure from the laser ablation of silicon targets maybe transform into ones with the zinc-blende structure in the plasma plume with the HTHPHD state by series crystal basal planes sliding.

During cooling down and condensation of the plasma plume in the confining liquid, the nucleation and growth of the zinc-blende silicon would occur. Meanwhile, the rapid quenching and growth time (about 20 ns in our case[54]) of the plasma plume leads to the synthesized metastable and stable phase frozen in the final products.[54] Additionally, the size of the final products usually in the range of micro- and nanometer scale due to the short quenching time.

There is a great influence of the inorganic salt ions in the plasma plume on the forming morphology of the synthesized cubes upon our PLIIR. The inorganic salt ions in the plasma plume could act as an oriented agent to induce the growth of the silicon nuclei due to the anisotropy in the adsorption stability of the salt ions. For the metastable nuclei with the cubic shape, the preferential adsorption lowers the surface energy of the bound plane and hinders the crystallite growth perpendicular to the plane, resulting in the final morphology of the synthesized products. Importantly, our relevant experimental studies (Figure 6) show that the inorganic salts have effects on the shape formation of the products upon our PLIIR. Otherwise, the usual single-crystalline nuclei with the stable phase would develop to the typical silicon balls. Additionally, our experiments above confirm that the amorphous carbon layer covered the silicon target has influence on the shape formation of silicon cubes in our synthesis. However, the detailed mechanisms are still

(59) Yang, G. W.; Wang, J. B. *Appl. Phys. A: Mater. Sci. Process.* **2001**, *72*, 475.

unclear. Thus, we will pursue the issue in our further study. An illustrative summary of the synthesis mechanism is depicted schematically in Figure 7.

IV. Conclusion

In summary, single-crystalline micro- and nanocubes of silicon with the zinc-blende structure, for the first time, have been synthesized by pulsed-laser-induced liquid–solid interface reaction assisted low-concentration inorganic salt solutions. Because of the unique shape and property, silicon cubes could be used as building blocks for fabrications of new nanodevices. Meanwhile, PLIIR could be expected to be a general route to synthesis other semiconductor micro- and nanocubes.

Acknowledgment. The National Natural Science Foundation of China (50525206 and 10474140) and the Ministry of Education (106126) funded this work.

CM7027178